On recurrent solutions within high-dimensional, non-dissipative Lorenz models: The role of the nonlinear feedback loop

B.-W. Shen* and S. Faghih-Naini

Department of Mathematics and Statistics
San Diego State University
5500 Campanile Drive
San Diego, CA, 92182, USA
*E-mail: bshen@mail.sdsu.edu; bowen.shen@gmail.com

Abstract. A recent study suggested that the nonlinear feedback loop of the three-dimensional, non-dissipative Lorenz model (3D-NLM) plays a role as a nonlinear restoring force in producing nonlinear oscillatory solutions, as well as linear periodic solutions near a non-trivial critical point. A follow-up study using the 5D-NLM examined the role of the extension of the nonlinear feedback loop in producing quasi-periodic solutions with two incommensurate frequencies. In this study, we analyze recurrent and quasi-periodic solutions within higher-dimensional NLMs (e.g., a 7D-NLM) with the goal of understanding how further extension of the nonlinear feedback loop may produce additional incommensurate frequencies.

While the nonlinear feedback loop of the 3D-NLM consists of a pair of downscaling and upscaling processes, the extended feedback loop within the 5D-NLM introduces two additional pairs of downscaling and upscaling processes, as compared to the 3D-NLM. Here, based on the extension of the nonlinear feedback loop within the 5D-NLM, we derive the 7D-NLM that has five pairs of downscaling and upscaling processes with three pairs that are the same as those within the 5D-NLM. In the 7D-NLM, the second and fourth pairs of downscaling and upscaling processes provide two-way interactions amongst the primary (the largest scale), secondary, and tertiary (the smallest scale) modes. By comparing the numerical simulations using one- and two-way interactions, we illustrate that proper representation of two-way interactions is crucial for capturing recurrent solutions with accurate incommensurate frequencies.

We also derive mathematical equations in order to provide an analogy between a linearized high-dimensional NLM and a system with different coupled springs. We show that the locally linear 7D-NLM (5D-NLM) is analogous to a system with three (two) different springs. This analogy can help illustrate how additional incommensurate frequencies may be generated by coupling additional springs with existing springs, indicating a similar impact between the coupling of springs and the extension of the nonlinear feedback loop. At the end, we outline future work designed for comparing various types of solutions for dissipative and non-dissipative LMs in order to understand whether steady-state, chaotic or limit torus solutions may better describe the nature of weather.

Keywords: downscaling and upscaling, Lorenz model, limit torus, nonlinear feedback loop, quasi-periodicity, recurrent solutions.

10^{th} *CHAOS Conference Proceedings, 30 May - 2 June, 2017, Barcelona, Spain*

1 Introduction

In 1963, Prof. Lorenz introduced a set of three ordinary differential equations (ODEs) for illustrating the nature of chaotic solutions that changed the view of atmospheric predictability [1–5]. The set of ODEs is now known as the three-dimensional Lorenz model (3DLM). Since chaotic solutions appear in the presence of nonlinearity within the 3DLM, the source of chaos has been suggested to be nonlinearity. The 3DLM was derived from partial differential equations (PDEs) that are the governing equations for the Rayleigh Benard convection [6,1]. In the original PDEs, three various types of physical processes are nonlinear interactions, heating, and dissipations. In our recent studies using high-dimensional LMs [7–13], we made an attempt at understanding the individual and/or collective impact of the above physical processes on the characteristics of solutions with the goal of extending the lead time for weather predictions [14,15]. For example, the 5D and 7D LMs were derived in order to illustrate the so-called negative nonlinear feedback in association with additional dissipative and nonlinear terms [7,11], while the 6D and 8D LMs were used in order to illustrate positive nonlinear feedback in association with additional heating and nonlinear terms [10,12]. Negative (positive) nonlinear feedback increases (decreases) the critical values for the Rayleigh parameter (i.e., the heating parameter) for the onset of chaos (see Table 1 in [12] for details). Recently, using 3D and 5D non-dissipative LMs that are conservative, we examined the collective impact of heating and nonlinearity on the appearance of recurrent (i.e., periodic or quasi-periodic to be specific) solutions [8,13]. As compared to other high-dimensional LMs [16,17], the strength of our high-dimensional LMs was documented in [7,10,11].

In the 3DLM, steady-state solutions and chaotic solutions appear at small and moderate values of the heating parameters, respectively. Additionally, limit cycle solutions may appear within the 3DLM with large heating parameters. A limit cycle (LC) is an isolated closed orbit near which no other closed orbits can be found. As a result of the isolated nature of the LC, an orbit, beginning at a point near the LC, will be attracted to the LC, indicating the independence of the LC solution on initial conditions (ICs). The unique characteristic of a LC solution implies better predictability as compared to a chaotic solution. By comparison, periodic or quasi-periodic orbits within non-dissipative LMs are not isolated and, thus, are dependent on the starting location. Therefore, a comparison of the LC within the dissipative LM and a quasi-periodic solution within the non-dissipative LM may provide a starting point for examining the role of small (moderate) dissipations in generating LC (chaotic) solutions. Note that when the limit cycle has two or more incommensurate frequencies, it is referred to as the limit torus that is quasi-periodic.

The paper is organized as follows: 1) We first provide an introduction to the topic; 2) In Section 2, we present mathematical equations for the 7D-NLM and for an analogy of the locally linear 7D-NLM to a system with different springs. 3) In Section 3, we discusses analytical solutions of incommensurate frequencies for the locally linear 7D-NLM and numerical solutions of the linear and nonlinear 7D-NLM. We also provide a mathematical comparison between

the 3D-NLM for periodic solutions and the 3DLM containing large heating parameters for LC solutions. We then present numerical solutions of the limit torus from high-dimensional LMs (e.g., the 5DLM and 7DLM with $r = 800$). 4) Concluding remarks are provided at the end.

2 The seven-dimensional, non-dissipative Lorenz Model

This section describes governing equations for the 7D-NLM and the corresponding locally linear 7D-NLM; and a mathematical analogy between the linearized 7D-NLM and a coupled system that contains three identical masses and three different springs.

By applying the same approach that was used to derive the 5D-NLM [7,13], we first obtain the 7DLM [11] and derive the 7D-NLM by removing the dissipative terms of the 7DLM, as follows:

$$\frac{dX}{d\tau} = \cancel{-\sigma X} + \sigma Y, \tag{1}$$

$$\frac{dY}{d\tau} = -XZ + rX - \cancel{Y}, \tag{2}$$

$$\frac{dZ}{d\tau} = XY - XY_1 - \cancel{bZ}, \tag{3}$$

$$\frac{dY_1}{d\tau} = XZ - 2XZ_1 - \cancel{d_\sigma Y_1}, \tag{4}$$

$$\frac{dZ_1}{d\tau} = 2XY_1 - 2XY_2 - \cancel{4bZ_1}, \tag{5}$$

$$\frac{dY_2}{d\tau} = 2XZ_1 - 3XZ_2 - \cancel{d_\sigma Y_2}, \tag{6}$$

$$\frac{dZ_2}{d\tau} = 3XY_2 - \cancel{9bZ_2}. \tag{7}$$

In the equations shown above, dissipative terms are indicated using a crossout symbol. As discussed in [11], $(X, Y, Z, Y_1, Z_1, Y_2, Z_2)$ represent the amplitude of the Fourier modes. We refer to (X, Y, Z) as the primary modes, (Y_1, Z_1) as the secondary modes, and (Y_2, Z_2) as the tertiary modes. τ is dimensionless time. The two parameters (σ, r) are the Prandtl number and the normalized Rayleigh number (or the heating parameter), respectively. Detailed information regarding these parameters and ignored terms is provided in [11]. The linear heating term (rX) and the nonlinear force terms (e.g., $-XZ$ and XY) appear on the right-hand side of the above equations.

By applying a perturbation method that represents the total field (A) as a sum of the reference state (A_c) and the perturbation (A') (i.e., $A = A_c + A'$), we transform Eqs. (1-7) into the following equations:

$$\frac{dX'}{d\tau} = \sigma Y', \tag{8}$$

$$\frac{dY'}{d\tau} = (r - Z_c)X' - X_c Z' - FN(X'Z'), \tag{9}$$

$$\frac{dZ'}{d\tau} = (Y_c - Y_{1c})\,X' + X_c Y' - X_c Y_1' + FN(X'Y' - X'Y_1'), \tag{10}$$

$$\frac{dY_1'}{d\tau} = (Z_c - 2Z_{1c})X' + X_c Z' - 2X_c Z_1' + FN(X'Z' - 2X'Z_1'), \tag{11}$$

$$\frac{dZ_1'}{d\tau} = (2Y_{1c} - 2Y_{2c})X' + 2X_c Y_1' - 2X_c Y_2' + FN(2X'Y_1' - 2X'Y_2'). \tag{12}$$

$$\frac{dY_2'}{d\tau} = (2Z_{1c} - 3Z_{2c})X' + 2X_c Z_1' - 3X_c Z_2' + FN(2X'Z_1' - 3X'Z_2'), \tag{13}$$

$$\frac{dZ_2'}{d\tau} = 3Y_{2c}X' + 3X_c Y_2' + FN(3X'Y_2'). \tag{14}$$

As discussed in [7,13], the flag FN is introduced in order to perform linear simulations ($FN = 0$) or nonlinear simulations ($FN = 1$). Equations (1-7) are referred to as the 7D-NLM V1 and Eqs. (8-14) are referred to as the 7D-NLM V2. The 7D-NLM V1 and V2 with $FN = 1$ should produce identical results with the same initial conditions, except in cases when rounding errors lead to different results in different models. The V2 with FN=0 is also referred to as the locally linear 7D-NLM and, as discussed in Section 3.1, can be used for a linear stability analysis. Four coupling terms form two pairs of downscaling processes (the terms shown above in black circles) and upscaling processes (the terms shown above in colored circles).

2.1 An analogy to a system with three coupled springs

Choosing $FN = 0$ and $(Y_c, Z_c, Y_{1c}, Z_{1c}, Y_{2c}, Z_{2c}) = (0, r, 0, \frac{r}{2}, 0, \frac{r}{3})$, we can obtain:

$$\frac{d^2Y'}{d\tau^2} = -X_c \frac{d^2Z'}{d\tau^2} = -X_c^2(Y' - Y_1') \tag{15}$$

from Eqs. (9-10),

$$\frac{d^2Y_1'}{d\tau^2} = X_c \frac{d^2Z'}{d\tau^2} - 2X_c \frac{d^2Z_1'}{d\tau^2} = X_c^2(Y' - 5Y_1' + 4Y_2') \tag{16}$$

from Eqs. (10-12), and

$$\frac{d^2Y_2'}{d\tau^2} = 2X_c \frac{d^2Z_1'}{d\tau^2} - 3X_c \frac{d^2Z_2'}{d\tau^2} = X_c^2(4Y_1' - 13Y_2') \tag{17}$$

from Eqs. (12-14).

For comparison with the 7D-NLM, we present governing equations for a coupled system containing three identical masses and three different springs, as shown in Figure 1c:

$$\frac{d^2x_1}{d\tau^2} = -k_1(x_1 - x_2), \tag{18}$$

$$\frac{d^2x_2}{d\tau^2} = -k_2(x_2 - x_3) - k_1(x_2 - x_1), \tag{19}$$

$$\frac{d^2x_3}{d\tau^2} = -k_3x_3 - k_2(x_3 - x_2). \tag{20}$$

The top, middle, and bottom springs have spring constants of k_3, k_2, and k_1, respectively. Here, the top spring is attached to the ceiling on one end and to the top mass on the other end. The upper (low) end of the middle spring is attached to the top (middle) mass. For the bottom spring, its upper (low) end is attached to the middle (bottom) mass. $x_1(\tau)$, $x_2(\tau)$, and $x_3(\tau)$ are the displacements of the centers of masses from equilibrium. By choosing $x_1 = Y', k_1 = X_c^2, x_2 = Y_1', k_2 = 4X_c^2, x_3 = Y_2'$, and $k_3 = 9X_c^2$, we show that Eqs. (18-20) are identical to Eqs. (15-17), respectively. In other words, the above coupled system with three springs is identical to the locally linear 7D-NLM. Note that for each of the uncoupled one-mass-one-spring systems, the frequency of oscillatory motion is either X_c, $2X_c$, or $3X_c$. By comparison, in section 3.1, we show that the above system has three frequencies, but they differ from the values of X_c, $2X_c$, or $3X_c$. More important, these frequencies are incommensurate, leading to a quasi-periodic solution. Since the 7D-NLM (5D-NLM) is derived by properly selecting new modes in order to extend the nonlinear feedback loop of the 5D-NLM (3D-NLM), the 7D-NLM can be reduced to become a 5D-NLM (3D-NLM) by removing the tertiary (both tertiary and secondary) modes, analogous to a system with two (one) springs, as shown in Figure 1.

In the next section, we discuss how the extended nonlinear feedback loop introduces two additional pairs of downscaling and upscaling processes that produce an additional temporal oscillatory mode and couple it with two existing temporal oscillatory modes.

3 Results

In this section, we present analytical solutions for eigenvalues with incommensurate frequencies within the locally linear 7D-NLM and numerical solutions for the 7D-NLM. We also briefly compare the quasi-periodic solutions within non-dissipative LMs and limit cycle solutions within dissipative LMs containing large heating parameters.

3.1 Eigenvalue analysis

Without a loss of generality, the reference (basic) state X_c is determined as:

$$X_c = \sqrt{X_o^2 + 49\sigma r/18} \tag{21}$$

based on the conservation of the normalized total energy. Here, X_o is an initial condition for the total field of X. For the remaining basic states, we choose $(Y_c, Z_c, Y_{1c}, Z_{1c}, Y_{2c}, Z_{2c}) = (0, r, 0, \frac{r}{2}, 0, \frac{r}{3})$. Plugging the above values into Eqs. 8 to 14 and setting $FN = 0$, the 7D-NLM system can be represented by a linear system with the following matrix:

$$A^{7D} = \begin{pmatrix} 0 & \sigma & 0 & 0 & 0 & 0 & 0 \\ 0 & 0 & -X_c & 0 & 0 & 0 & 0 \\ 0 & X_c & 0 & -X_c & 0 & 0 & 0 \\ 0 & 0 & X_c & 0 & -2X_c & 0 & 0 \\ 0 & 0 & 0 & 2X_c & 0 & -2X_c & 0 \\ 0 & 0 & 0 & 0 & 2X_c & 0 & -3X_c \\ 0 & 0 & 0 & 0 & 0 & 3X_c & 0 \end{pmatrix} \tag{22}$$

By applying Laplace's formula and by expressing the determinant as determinants of minors leads to the following equation:

$$\lambda^7 + 19\lambda^5 X_c^2 + 66\lambda^3 X_c^4 + 36\lambda X_c^6 = 0. \tag{23}$$

As easily seen, one eigenvalue must be zero. By setting $\gamma = \lambda^2$, the following nonlinear equation of the third order must be solved in order to obtain the remaining eigenvalues:

$$\gamma^3 + 19\gamma^2 X_c^2 + 66\gamma X_c^4 + 36 X_c^6 = 0, \tag{24}$$

which yields:

$$\gamma = \left(-\frac{19}{3} - \frac{163(1+i\sqrt{3})}{6\sqrt[3]{-1702+27i\sqrt{1967}}} - \frac{1}{6}(1-i\sqrt{3})\sqrt[3]{-1702+27i\sqrt{1967}} \right) X_c^2,$$

$$\gamma = \left(-\frac{19}{3} - \frac{163(1-i\sqrt{3})}{6\sqrt[3]{-1702+27i\sqrt{1967}}} - \frac{1}{6}(1+i\sqrt{3})\sqrt[3]{-1702+27i\sqrt{1967}} \right) X_c^2 \text{ and}$$

$$\gamma = \left(-\frac{19}{3} + \frac{1}{3}\left(\frac{163}{\sqrt[3]{-1702+27i\sqrt{1967}}} + \sqrt[3]{-1702+27i\sqrt{1967}} \right) \right) X_c^2. \tag{25}$$

The above expressions yield three different incommensurate frequencies, whose numerical values are obtained from the imaginary parts of the following eigenvalues: $\lambda_1 \approx i(0.818657)X_c$ $\lambda_2 = -\lambda_1$, $\lambda_3 \approx i(1.91368)X_c$, $\lambda_4 = -\lambda_3$, $\lambda_5 \approx i(3.82983)X_c$, $\lambda_6 = -\lambda_5$, and $\lambda_7 = 0$. By comparison, the non-zero eigenvalues of the 5D-NLM are $\approx \pm i(0.874032)X_c$ and $\approx \pm i(2.288246)X_c$. In the next section, the three frequencies in Eq. (25) will be used as theoretical values for a comparison to the numerical results.

3.2 Numerical results

For numerical integrations, the parameters $\sigma = 10$ and $b = 8/3$ are kept constant. The heating parameter is $r = 25$ for quasi-periodic solutions of the non-dissipative LMs and $r = 800$ for LC solutions of the dissipative LMs. A dimensionless time interval ($\triangle\tau$) of 0.001 is used.

Figures 2a-d show the time evolution of solutions for the X', Y' (primary), Y_1' (secondary), and Y_2' (tertiary) modes. Figures 2e-h display the corresponding spectral analysis. Analytical solutions of the eigenvalues are shown with green, blue, and red lines, denoted as theoretical values of high, moderate, and low frequencies, respectively. For the primary modes (X' or Y'), two prominent frequencies exist. The two corresponding peaks within the spectrum display good agreement with the analytical solution of eigenvalues indicated with blue and red lines. In the numerical results, the low frequency mode has a much larger amplitude than the moderate frequency mode. Thus, the time evolution of primary modes appears almost periodic. For the secondary mode (Y_1'),

two prominent frequencies can also be observed. The moderate-frequency mode has an amplitude that is approximately 1/3 the amplitude of the low-frequency mode. Therefore, the secondary mode appears quasi-periodic with the two frequencies. The results are consistent with findings within the 5D-NLM (see details in [13]). In addition to the primary and secondary modes that also appear within the 5D-NLM, a tertiary mode (Y_2') is included within the 7D-NLM and an additional incommensurate frequency appears within the corresponding locally linear 7D-NLM. Figure 2h provides the spectrum of the tertiary mode containing three prominent frequencies that are consistent with analytical solutions of the eigenvalues. The low-frequency mode has the largest amplitude and the high-frequency mode has the smallest amplitude. As a result of the three prominent frequencies, the tertiary mode appears to be the most "irregular" solution as compared to the primary and secondary modes.

The impact of nonlinearity on the quasi-periodicity of the solution is discussed in Figure 3. Nonlinear and linear solutions have comparable amplitudes, but different phases (Figure 3a). In Figure 3b, as indicated by the peaks of black dots, three prominent frequencies appear within the nonlinear solution. The low and moderate frequencies are in good agreement with the linear theoretical values, while the high frequency has a larger discrepancy as compared to the theoretical value (in green). The 7DLM (as well as the 7D-NLM) was derived based on an extension of the nonlinear feedback loop of the 5DLM. As shown in Eq. 22, the role of the extended nonlinear feedback loop can be illustrated using the matrix of the linearized model. For example, when the coupling terms in the red and blue boxes are ignored (i.e., resetting these terms to zero), the system contains three frequencies, X_c, $2X_c$, and $3X_c$, that are not incommensurate. Namely, the inclusion of tertiary modes, based on the extension of the nonlinear feedback loop, introduces an additional (high) frequency that is incommensurate with the existing frequencies (i.e., low and moderate frequencies).

The role of the extended nonlinear feedback loop in producing quasi-periodic solutions may be illustrated by ignoring some or all of the coupling terms in the numerical solutions. Using the 5D-NLM [13], we previously examined the impact of two-way and one-way interactions on the quasi-periodicity of solutions containing two incommensurate frequencies. Using the 7D-NLM, for this study, we focus on the impact of one-way interactions that provide downscaling transfer from larger-scale processes to smaller-scale processes but that do not provide upscaling transfer from smaller-scale processes to larger-scale processes. In other words, one or two of the coupling terms in red or blue circles may be ignored while coupling terms in black circles are kept in Eqs. 8-14. When the coupling term in Eq. 10 shown in a red circle is neglected, the secondary modes (as well as the tertiary modes) cannot provide feedback to the primary modes. When the coupling term shown in the blue circle is ignored in Eq. 12, there is still a two-way interaction between the primary and secondary modes, but only a one-way interaction between the secondary and tertiary modes. In Fig. 4, the $Y-Z$ cross sections display a quasi-periodic solution containing three incommensurate frequencies for the control run for all coupling terms (panel a), a periodic solution for a parallel run with X_cY_1' ignored

in Eq. 10 (panel b), and a quasi-periodic solution containing two incommensurate frequencies for another parallel run with $2X_cY_2'$ ignored in Eq. 12 (panel c). For one-way coupling without the coupling term in Eq. (12), Eqs. 13-14 describe the time evolution of the tertiary modes $(Y_2 - Z_2)$ with an "external" forcing of $2X_cZ_1'$ that is enabled by the downscaling transfer of the secondary mode (Z_1'). Therefore, for this run, while the primary mode solutions $(Y - Z)$ display a quasi-periodic solution with two incommensurate frequencies (panel c), the tertiary mode solutions $(Y_2' - Z_2')$ display a quasi-periodic orbit with three frequencies (panel d). Note that the three frequencies are not exactly the same as those within the fully coupled system (e.g., Eq. 25). The above discussions suggest the importance of proper coupling for producing accurate, quasi-periodic solutions.

3.3 A comparison to the 3DLM using a large r

For the 3DLM with a large r, a multiscale analysis leads to the following approximate equations [18]:

$$\frac{\mathrm{d}X}{\mathrm{d}\tau} = \sigma Y, \tag{26}$$

$$\frac{\mathrm{d}Y}{\mathrm{d}\tau} = -XZ, \tag{27}$$

$$\frac{\mathrm{d}Z}{\mathrm{d}\tau} = XY. \tag{28}$$

The above equations are identical to the 3D-NLM with r=0 (e.g., Eqs. (1-3) with $Y_1 = 0$). While the 3DLM with a large r yields an isolated nonlinear oscillatory solution that is independent of the initial conditions (as shown in Fig. 5a), the approximate system (e.g., Eqs. 26-28) produces nonlinear oscillatory orbits that are dependent of their starting points [8]. In the former system, the isolated closed solution is a limit cycle solution. By comparison, while a high-dimensional NLM produces a quasi-periodic solution with incommensurate frequencies that appears as a torus, high-dimensional dissipative LMs with a large r produce limit torus solutions (i.e., LC solutions with incommensurate frequencies), as shown in Fig. 5. As discussed in Fig. 4 and in [13], the quasi-periodicity of solutions is better shown within the secondary or tertiary modes instead of the primary modes (as shown in the bottom panels of Fig. 5). Therefore, isolated orbits within high-dimensional LMs with large heating parameters are referred to as limit torus solutions. In addition to an isolated nature, one of the major differences between a limit torus within a dissipative LM at a larger r and the (regular) torus within the corresponding non-dissipative LM is that the time change of total energy varies along the limit torus.

4 Conclusions

For this study, we analyze and compare the recurrent (e.g., periodic or quasi-periodic) solutions in higher-dimensional NLMs (e.g., the 5D-NLM and the 7D-

NLM) with the goal of understanding the role of the extended nonlinear feedback loop (as well as the coupling terms) in producing additional incommensurate frequencies. While the 5D-NLM (3D-NLM) produces a quasi-periodic (periodic) solution with two incommensurate frequencies (one frequency), the 7D-NLM, with an extended nonlinear feedback loop, yields quasi-periodic solutions with three incommensurate frequencies. The 7D-NLM extends the nonlinear feedback loop of the 5D-NLM and has five pairs of downscaling and upscaling processes. The second and fourth pairs of downscaling and upscaling processes, referred to as the coupling terms, provide two-way interactions amongst the primary (the largest scale), secondary, and tertiary (the smallest scale) modes. Accurate representation of the two-way interactions is crucial for capturing accurate recurrent solutions containing accurate incommensurate frequencies. For example, results obtained using a one-way coupling in Figs. 4c-d indicate quasi-periodic solutions that contain two frequencies for the primary and secondary modes, but three frequencies for the tertiary modes. These frequencies are not exactly the same as those obtained within a fully coupled system (e.g., Eq. 25).

The importance of the coupling terms is further shown using mathematical equations that provide an analogy between a linearized, high-dimensional NLM and a system containing various coupled springs. We provide evidence that the 7D-NLM (5D-NLM) is analogous to a system containing three (two) different springs. The analogy indicates similarity between extending the nonlinear feedback loop and coupling additional springs with existing springs.

While non-dissipative LMs produce periodic or quasi-periodic solutions, dissipative LMs with large heating parameters yield limit cycle (or limit torus) solutions. The comparison suggests that: (1) the recurrence of solutions is associated with the nonlinear feedback loop and its extension; and (2) the isolated nature of a limit cycle (or limit torus) is associated with the inclusion of small dissipation. Amongst the various types of solutions (e.g., chaotic and LC solutions) within the 3DLM, chaotic solutions containing positive Lyapunov exponents [19] have been widely used for illustrating the characteristics of weather that never repeats. High-dimensional LMs also contain various types of solutions, including limit torus solutions that possess quasi-periodicity and non-zero growth rates. For our future work, we will systematically examine various types of solutions (e.g., by computing the time change for total energy along an orbit) using high-dimensional LMs (including a 9DLM) in order to understand whether a steady-state, chaotic, or limit torus solution may better describe the nature of weather.

Acknowledgements

We are grateful for support from the College of Science at San Diego State University. Resources supporting this work were provided by the NASA High-End Computing (HEC) program and the NASA Advanced Supercomputing division at Ames Research Center.

References

1. Lorenz, E.: Deterministic nonperiodic flow, J. Atmos. Sci., 20, 130–141, 1963.
2. Lorenz, E.: Predictability: does the flap of a butterfly's wings in Brazil set off a tornado in Texas?, in: American Association for the Advancement of Science, 139th Meeting, 29 December 1972, Boston, Mass., AAAS Section on Environmental Sciences, New Approaches to Global Weather, GARP, available at: http://eaps4.mit.edu/research/Lorenz/Butterfly_1972.pdf, last access: 14 December 2015, 1972.
3. IPCC: Climate Change 2007: The Physical Science Basis, in: Contribution of Working Group I to the Fourth Assessment Report of the Intergovernmental Panel on Climate Change, edited by: Solomon, S., Qin, D., Manning, M., Chen, Z., Marquis, M., Averyt, K. B., Tignor, M., and Miller, H. L., Cambridge University Press, Cambridge, UK and New York, NY, USA, 996 pp.
4. Pielke, R.: The Real Butterfly Effect, available at: http://pielkeclimatesci.wordpress.com/2008/04/29/the-real-butterfly-effect/, last access: 14 December 2015, 2008.
5. Anthes, R.: Turning the tables on chaos: is the atmosphere more predictable than we assume?, UCAR Magazine, spring/summer, available at: https://www2.ucar.edu/atmosnews/opinion/turning-tables-chaos-atmosphere-more-predictable-we-assume-0 (last access: 3 January 2016), 2011.
6. Saltzman, B.: Finite amplitude free convection as an initial value problem, J. Atmos. Sci., 19, 329–341, 1962.
7. Shen, B.-W.: Nonlinear feedback in a five-dimensional Lorenz model, J. Atmos. Sci., 71, 1701–1723, doi:10.1175/JAS-D-13-0223.1, 2014.
8. Shen, B.-W.: On the nonlinear feedback loop and energy cycle of the non-dissipative Lorenz model. Nonlin. Processes Geophys. Discuss., 1, 519-541, doi:10.5194/npgd-1-519-2014, 2014.
9. Shen, B.-W.: Parameterization of Negative Nonlinear Feedback using a Five-dimensional Lorenz Model, Fractal Geometry and Nonlinear Analysis in Medicine and Biology, 1, 33–41, doi:10.15761/FGNAMB.1000109, 2015a.
10. Shen, B.-W.: Nonlinear feedback in a six dimensional Lorenz model: impact of an additional heating term, Nonlin. Processes Geophys., 22, 749-764, doi:10.5194/npg-22-749-2015, 2015b.
11. Shen, B.-W.: Hierarchical scale dependence associated with the extension of the nonlinear feedback loop in a seven-dimensional Lorenz model. Nonlin. Processes Geophys., 23, 189-203, doi:10.5194/npg-23-189-2016, 2016.
12. Shen, B.-W.: On an extension of the nonlinear feedback loop in a nine-dimensional Lorenz model. Chaotic Modeling and Simulation (CMSIM). (accepted, December 15, 2016), 2016.
13. Faghih-Naini, S. and B.-W. Shen, 2017: On quasi-periodic solutions associated with the extended nonlinear feedback loop in the five-dimensional non-dissipative Lorenz model. The 10th Chaos Modeling and Simulation International Conference (CHAOS2017), Barcelona, Spain, 30 May - 2 June, 2017.
14. Shen, B.-W., Atlas, R., Reale, O., Lin, S.-J., Chern, J.-D., Chang, J., Henze, C., and Li, J.-L.: Hurricane forecasts with a global mesoscale-resolving model: Preliminary results with Hurricane Katrina (2005), Geophys. Res. Lett., 33, L13813, doi:10.1029/2006GL026143, 2006.
15. Shen, B. W., DeMaria, M., Li, J.-L. F., and Cheung, S.: Genesis of hurricane Sandy (2012) simulated with a global mesoscale model, Geophys. Res. Lett., 40, 4944–4950, doi:10.1002/grl.50934, 2013.

16. Curry, J. H., Herring, J. R., Loncaric, J., and Orszag, S. A.: Order and disorder in two- and three-dimensional Benard convection, J. Fluid. Mech., 147, 1–38, 1984.
17. Roy, D. and Musielak, Z. E.: Generalized Lorenz models and their routes to chaos, I. Energy-conserving vertical mode truncations, Chaos Soliton. Fract., 32, 1038–1052, 2007.
18. Sparrow, C.: The Lorenz Equations: Bifurcations, Chaos, and Strange Attractors. Springer, New York. Appl. Math. Sci., 41, 1982.
19. Wolf, A., Swift, J. B., Swinney, H. L., and Vastano, J. A.: Determining Lyapunov exponents from a time series, Physica, 16, 285–317, 1985.

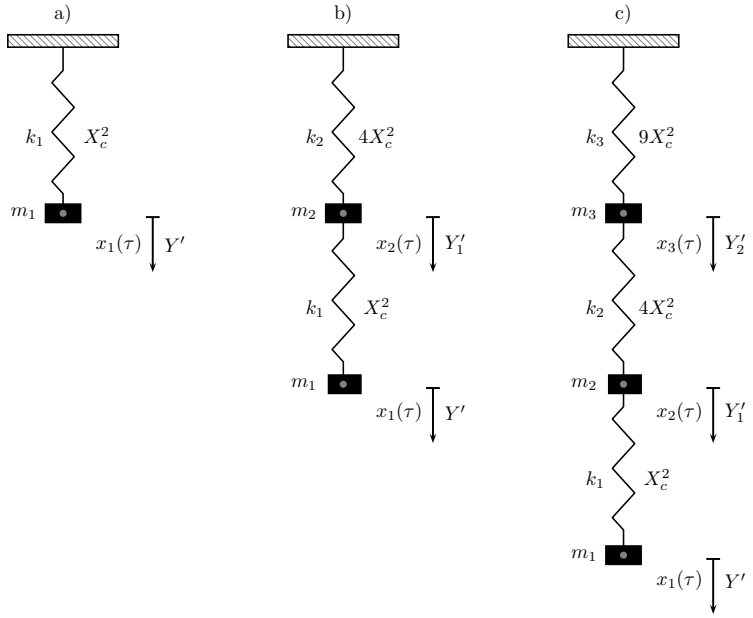

Figure 1: Systems with one mass and one spring (a), two masses and two springs (b), and three masses and three springs (c). The three masses are identical (i.e., $m_1 = m_2 = m_3$). Three spring constants, k_1, k_2 and k_3, are selected as X_c^2, $4X_c^2$, and $9X_c^2$, respectively. The governing equations for the above systems in panels (a)-(c) are identical to those for the locally linear 3D-NLM, 5D-NLM, and 7D-NLM, respectively. The comparison illustrates how the nonlinear feedback loop and its extension, enabled by the proper selection of high wavenumber modes, can produce recurrent (i.e., periodic or quasi-periodic) solutions.

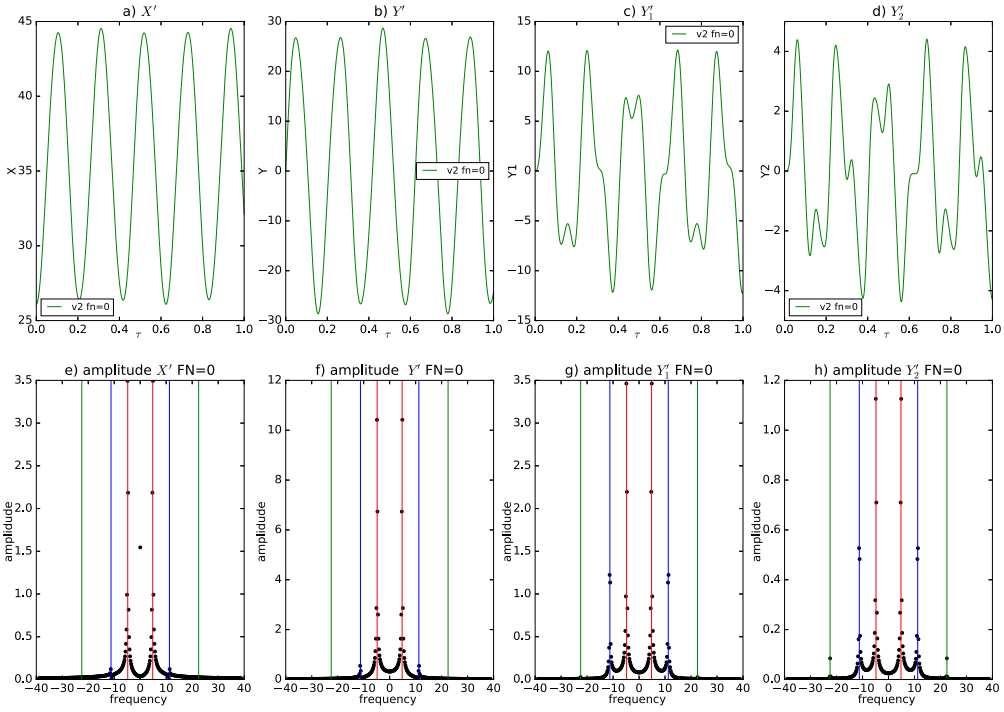

Figure 2: The time evolution of solutions for the primary, secondary and tertiary modes (i.e., Y, Y_1' and Y_2') for $\tau \in [0, 1.0]$ from the locally linear 7D-NLM. Panels (a-d) display X', Y', Y_1', and Y_2', respectively. Panels (e-h) provide the corresponding frequency analysis. The analytical solutions of eigenvalues for high, moderate, and low frequencies are shown with green, blue, and red lines, respectively. The tertiary mode (Y_2'), with the smallest spatial scale, displays three prominent incommensurate frequencies appearing to be the most "irregular" solution (right panels).

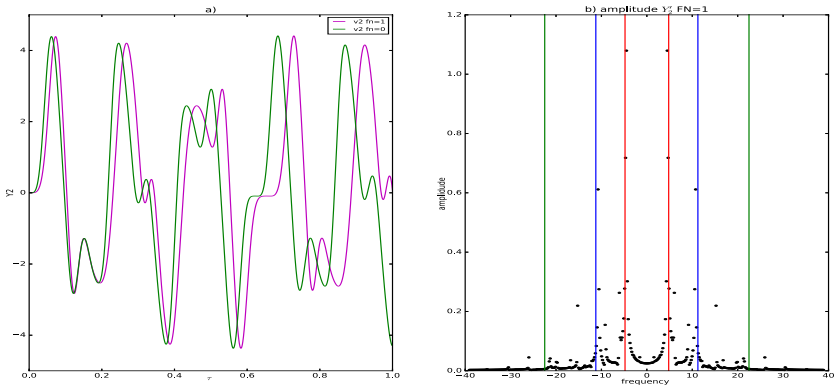

Figure 3: A comparison of the linear ($FN = 0$) and nonlinear ($FN = 1$) solutions (a). A frequency analysis of the nonlinear solution (b). The analytical solutions of eigenvalues for high, moderate, and low frequencies are shown with green, blue, and red lines, respectively.

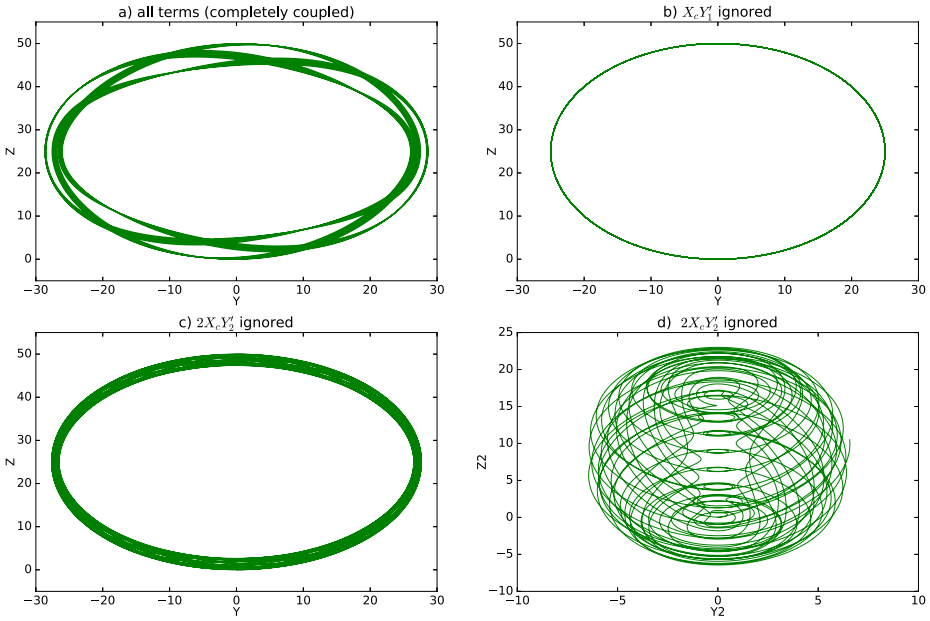

Figure 4: The impact of the coupling terms (i.e., one-way interaction, to be specific) on the quasi-periodicity of solutions within 7D-NLM V2 with FN=0. Panels (a-c) display the Y-Z cross section and panel (d) displays the $Y_2 - Z_2$ cross section. (a) A quasi-periodic solution with three incommensurate frequencies from the model. (b) A periodic solution with the coupling term X_cY_1' ignored in Eq. (10). (c) A quasi-periodic solution with two incommensurate frequencies for the primary mode solutions when upscaling processes from the tertiary modes are disabled by ignoring the coupling term $2X_cY_2'$ in Eq. (12). (d) A quasi-periodic solution with three frequencies for the tertiary mode solution resulting from a one-way downscaling transfer enabled by the coupling term $2X_cY_2'$ in Eq. (13).

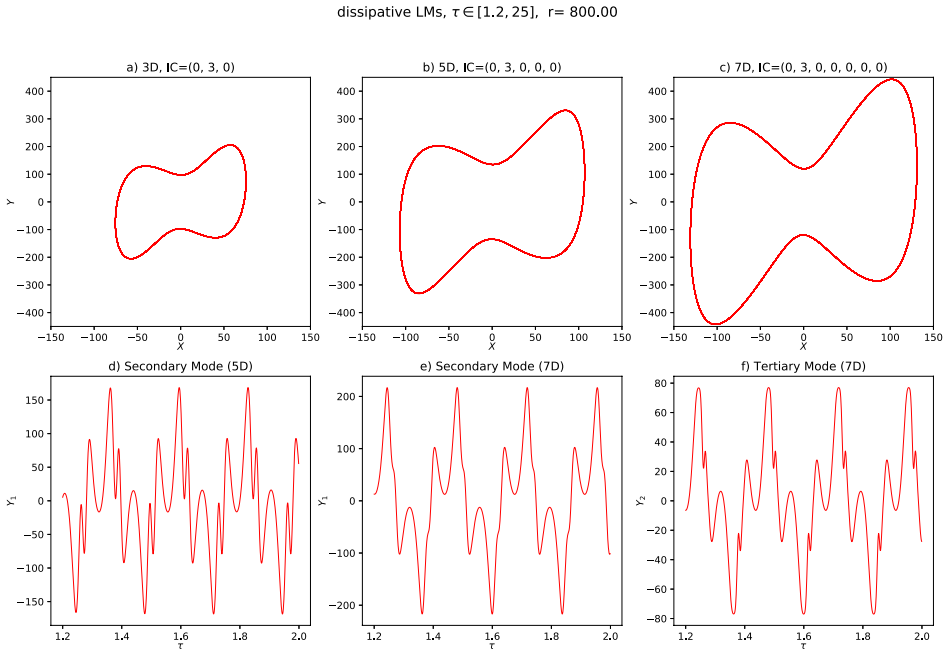

Figure 5: Limit cycle solutions within the 3DLM (a), 5DLM (b), and 7DLM (c) with r=800. Solutions for the period of $\tau = 1.2 - 25$ are provided. Panels (d)-(f) show the time evolution of the quasi-periodic solutions for $\tau \in [1.2, 2.2]$ for the secondary mode (Y_1') of the 5DLM, the secondary mode (Y_1') of the 7DLM, and the tertiary mode (Y_2') of the 7DLM, respectively.